Line tension of sessile droplets: Thermodynamic considerations

Haodong Zhang [1,2] Fei Wang [1,2,*] and Britta Nestler[1,3]
[1]*Institute of Applied Materials-Microstructure Modelling and Simulation, Karlsruhe Institute of Technology (KIT), Strasse am Forum 7, Karlsruhe 76131, Germany*
[2]*Institute of Nanotechnology, Karlsruhe Institute of Technology (KIT), Hermann-von-Helmholtz-Platz 1, Eggenstein-Leopoldshafen 76344, Germany*
[3]*Institute of Digital Materials Science, Karlsruhe University of Applied Sciences, Moltkestrasse 30, Karlsruhe 76133, Germany*

We deduce a thermodynamically consistent diffuse interface model to study the line tension phenomenon of sessile droplets. By extending the standard Cahn-Hilliard model via modifying the free energy functional due to the spatial reflection asymmetry at the substrate, we provide an alternative interpretation for the wall energy. In particular, we find the connection of the line tension effect with the droplet-matrix-substrate triple interactions. This finding reveals that the apparent contact angle deviating from Young's law is contributed by the wall energy reduction as well as the line energy minimization. Besides, the intrinsic negative line tension resulting from the curvature effect is observed in our simulations and shows good accordance with recent experiments [Tan *et al.* Phys. Rev. Lett. **130**, 064003 (2023)]. Moreover, our model sheds light upon the understanding of the wetting edge formation which results from the vying effect of wall energy and line tension.

I. INTRODUCTION

The line tension effect describes the apparent contact angle θ of a sessile droplet influenced by the energy contribution at the triple junction which is a 2D geometrical line, where the droplet meets the surrounding fluid on a solid substrate, see Fig. 1(a) [1–3]. Gibbs first heeded the thermodynamics of the line tension in his theory of capillarity [4]. Later on, Tolman derived the surface tension σ_{LV} of the droplet depending on the droplet cap radius R as [5]

$$\sigma_{LV}(R) = \sigma_{LV}^{\infty}\left(1 - \frac{2\,\delta_T}{R}\right), \tag{1}$$

where σ_{LV}^{∞} is the surface tension for a planar interface and the Tolman length δ_T decides the magnitude of the line tension. In this way, the modified Young's law reads

$$\cos\theta = \cos\theta_Y - \frac{\gamma_T}{\sigma_{LV}^{\infty}\, r^*} + \mathcal{O}\left(\frac{1}{r^{*2}}\right). \tag{2}$$

Here, $r^* = R\sin\theta$ is the base radius of the contact line. The line tension γ_T is engendered by curvature-dependent surface tension, so that the apparent contact angle θ approaches Young's contact angle θ_Y as $r^* \to \infty$. A similar formulation is also obtained by Widom [6], resulting from the minimization of the surface and line energies. The inverse relationship between $\cos\theta$ and r^* indicates that the line tension effect has a magnificent impact not only on the submicro scale droplets, such as surface nucleation [7] and droplet spreading [8], but also on the stability of nanobubbles/particles [9,10]. Other applications, such as lipid membrane manufacture [11] and the cell manipulation [12] also demand a better understanding on the line tension. Especially, the magnitude and the sign of the line tension are still a knotty issue. The positive line tension [13,14] is reported ranging from several pJ/m to μJ/m. However, a negative line tension with an absolute value much greater than 1.0 nJ/m is very seldom measured in experiment [15].

In this work, we provide a detailed elucidation of the line tension effect utilizing a thermodynamically consistent diffuse interface model in Sec. II. This model extends the Cahn-Hilliard theory adopted in Ref. [16] by formulating a comprehensive wall free energy functional, containing a local wall energy term and a nonlocal line energy term within the wetting layer. We will explore the positive line tension in Sec. III A, while also observing instances of weak negative line tension. Notably, leveraging our model, we delineate the presence of a negative line tension from the mathematical and thermodynamical standpoint. Furthermore, the underlying mechanism governing the wetting edge formation through the influence of line tension is thoroughly analyzed in Sec. III B. Distinct from the conventional sharp interface approach, we assert that the wetting phenomenon with the line tension is not solely predicated upon the properties of the droplet-matrix binary system. Instead, we posit that it constitutes a multifaceted problem. By considering the intricate triple interaction involving the droplet, matrix, and substrate through the wall energy functional, we demonstrate that the establishment of Young's contact angles with the line tension effect emerges as a delicate interplay between the competing mechanisms of wall energy reduction and line energy minimization, rather than being solely attributed to line tension.

*fei.wang@kit.edu

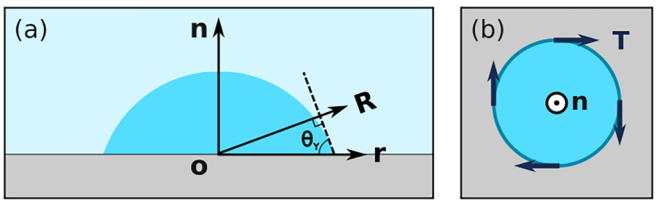

FIG. 1. (a) A sessile droplet on a flat solid substrate with Young's contact angle θ_Y. The vectors $\mathbf{R}, \mathbf{n}, \mathbf{r}$ direct the normal direction of the droplet cap of the substrate and of the contact line, respectively. (b) The bird's eye view of the dark blue line tension vectors $\mathbf{T}$ tangent to the mid-blue contact line.

II. MODEL DESCRIPTION

In this section, we present the diffuse-interface line tension model. We consider a droplet on a solid substrate S. The local volume concentration of the liquid phase is denoted by c which is space $\boldsymbol{x}$ and time t dependent in the domain Ω. In the standard Cahn-Hilliard approach, the free energy of a nonuniform system reads

$$F(c, \nabla c) = \int_\Omega [f(c) + \boldsymbol{L} \cdot \nabla c + \kappa (\nabla c)^2 + \dots] d\Omega,$$

where f(c) describes the bulk free energy density and κ is the gradient energy coefficient. For isotropic systems, the odd order term of ∇c is canceled ($\boldsymbol{L} = \boldsymbol{0}$) due to its invariance to the reflection symmetry operation ($\boldsymbol{x}$ to $-\boldsymbol{x}$) [17]. However, for the sessile droplet contacting the solid substrate, this reflection symmetry breaks on the substrate. Particularly, the system becomes dependent on the reflection operation $\boldsymbol{n}$ to $-\boldsymbol{n}$ in the normal direction of the substrate surface (see Fig. 1). Hence, we add two ∇c-related terms in the free energy functional of the domain Ω as

$$\mathcal{F} = \int_\Omega [f(c) + \kappa (\nabla c)^2 + \kappa_1 \nabla c \cdot \boldsymbol{n} + 2\kappa^* \nabla^2 c \, \nabla c \cdot \boldsymbol{n}] d\Omega. \quad (3)$$

The fluid bulk free energy density $f(c)$ takes the regular solution formulation as [18]

$$f(c) = \frac{R_g T}{v_m} [c \ln c + (1-c) \ln(1-c) + \chi \, c \, (1-c)], \quad (4)$$

in which R_g, T, and v_m stand for the gas constant, temperature, and molar volume, respectively. The intermolecular interaction between droplet and matrix is scaled by the Flory parameter χ.

The physical meaning of the gradient energy coefficients κ_1 and κ^* is elucidated as follows. By assuming κ_1 to be the derivative of wall energy density $g(c)$ to the composition c, namely $\kappa_1 = dg/dc$, we rewrite the new terms in Eq. (3) as $\kappa_1 \nabla c \cdot \boldsymbol{n} + 2\kappa^* \nabla^2 c \, \nabla c \cdot \boldsymbol{n} = \nabla g \cdot \boldsymbol{n} + 2\kappa^* \nabla^2 c \, \nabla c \cdot \boldsymbol{n}$. For a flat solid substrate, the mean curvature is zero which leads to $\nabla \cdot \boldsymbol{n} = 0$. In fact, the following deduction is also valid for substrates with any geometrical shape, as proven in Appendix B. With this relationship, the κ_1 and κ^* related terms are further simplified as $\kappa_1 \nabla c \cdot \boldsymbol{n} + 2\kappa^* \nabla^2 c \, \nabla c \cdot \boldsymbol{n} = \nabla \cdot [g\boldsymbol{n} + \kappa^* (\nabla c)^2 \boldsymbol{n}]$. By applying the divergence theorem and using the no-flux boundary condition, the volume integration is transformed into the surface integral. After the standard calculus, we obtain the following wall energy formulation

$$\int_\Omega \nabla \cdot [g\boldsymbol{n} + \kappa^* (\nabla c)^2 \boldsymbol{n}] \, d\Omega = \int_S [g(c) + \kappa^* (\nabla c)^2] \, dS. \quad (5)$$

Noteworthily, the wall energy formulation of Eq. (5) differs from previous works [16,19] for studying the wetting effect. Therefore, the free energy functional $\mathcal{F}$ of the whole system reads

$$\mathcal{F} = \int_\Omega [f(c) + \kappa \, (\nabla c)^2] d\Omega + \int_S [g(c) + \kappa^* (\nabla c)^2] \, dS. \quad (6)$$

At equilibrium, the droplet-matrix interface tension [16] is expressed as

$$\sigma_{LV} = \int_{c_1}^{c_0} 2\sqrt{\kappa \, \Delta f} \, dc, \quad (7)$$

in which the excessive energy density Δf is defined as $f(c) - f(c_1) - (\partial f/\partial c - 2\kappa \nabla^2 c)(c - c_1)$. The limits of integration c_0 and c_1 stand for the equilibrium compositions of matrix and droplet, respectively. In this work, the surface tension parameter κ is fixed as two which is nondimensionalized by 10^{-11}N. The Flory parameter $\chi = 3.78$ is selected in Eq. (4) to model immiscible fluids having two local minima. Substituting $\chi = 3.78$ into f of Eq. (4), we ensure the interfacial tension Eq. (7) to be 1.0.

Adopting the Cahn-Hilliard type of phase-field model [19,20], the governing equations for the wetting phenomenon with the line tension effect are written as (see the derivation in Appendix A)

$$\frac{\partial c}{\partial t} == \nabla \cdot \left[\mathcal{M} \nabla \left(\frac{\partial f}{\partial c} - 2\kappa \nabla^2 c \right) \right] \qquad \text{in}\Omega, \quad (8)$$

$$\frac{\partial c}{\partial t} = \tau \left(2\kappa \nabla c \cdot \mathbf{n} - g' + 2\kappa^* \nabla_s^2 c \right) \qquad \text{on } S, \quad (9)$$

where the surface Laplacian is defined as $\nabla_s^2 c := \nabla^2 c - \nabla(\nabla c \cdot \mathbf{n}) \cdot \mathbf{n}$. The mobility $\mathcal{M} = (v_m / R_g T) D_0 c \, (1-c)$ follows the Onsager's reciprocal relation [21,22] with the interdiffusivity $D_0 = 1$ normalized by the characteristic diffusivity 10^{-9} m^2/s. The phenomenological parameter τ determines the deviation of the system from the equilibrium state [19] and is set as 0.01 (equivalent to 10^8 s/kg) in this work.

The wall energy density g takes the double well potential (a quartic function as [23])

$$g(c) = s \frac{(c - c_0)^2 (c - c_1)^2}{4} - \alpha \left(\frac{c^3}{3} - \frac{c^2}{2} + c_0 c_1 c \right) + \text{C}, \quad (10)$$

where s is the scaling factor for the droplet-matrix-substrate triple interaction and C is a constant. Since the surface equilibrium compositions solved by Eq. (9) are identical to the bulk composition obtained by Eq. (8), the term $g'(c)$ ought to be zero at two equilibrium compositions; see Fig. 5(b) and Ref. [24]. Taking the parabolic function for $g'(c) = \alpha(c - c_0)(c - c_1)$ and applying the constraint $g(c_1) - g(c_0) = \sigma_{LS} - \sigma_{SV}$, we have $\alpha = 6 \cos\theta_Y / (c_1 - c_0)^3$. Integrating the wetting boundary condition with the derived factor α leads to

$$\sigma_{LS} - \sigma_{SV} = g(c_1) - g(c_0) = \sigma_{LV} \cos\theta_Y.$$

Here, σ_{LS} denotes the droplet-substrate interfacial tension, and σ_{SV} depicts the matrix-substrate interfacial tension. More

validation and theoretical analyses of this approach can be found in Ref. [16].

Next, to recover the modified Young's law at equilibrium, the equilibrium condition Eq. (9) by setting $\partial c/\partial t = 0$ is integrated from the equilibrium composition c_1 to c_0 in the polar coordinate as

$$\begin{aligned}\int_{c_1}^{c_0} \left(2\kappa \nabla c \cdot \mathbf{n} - g' + 2\kappa^* \nabla_s^2 c\right) dc \\ = \int_0^{\infty} 2\kappa (\partial_R c)^2 \cos\theta \, dR - \int_{c_1}^{c_0} \left[g' - 2\kappa^* \left(\frac{\partial_r c}{r} + \partial_{rr} c\right)\right] dc \\ = \sigma_{LV} \cos\theta + \sigma_{SV} - \sigma_{LS} + \frac{\gamma}{r^*} = 0. \end{aligned} \tag{11}$$

By using the calculus of integration by parts, the integral of the Laplacian term vanishes,

$$\int_{c_0}^{c_1} 2\,\kappa^* \partial_{rr} c \, dc \equiv 0, \tag{12}$$

and makes no contribution to the line tension of the sharp contact line, but this Laplacian term cannot be neglected and highlights the crucial difference between the sharp and diffuse interface models of the line tension, as will be demonstrated in next section. Most importantly, we obtain the first-order approximation of the line energy density in the diffuse interface model

$$\gamma = \int_0^{\infty} 2\kappa^* (\partial_r c)^2 dr. \tag{13}$$

Finally, substituting the Tolmann equation Eq. (1) into Eq. (11), we derive the modified Young's equation with the line tension effect as

$$\cos\theta = \cos\theta_Y - \frac{\gamma + \gamma_T}{\sigma_{LV}^{\infty} r^*} + \mathcal{O}\left(\frac{1}{r^{*2}}\right). \tag{14}$$

III. RESULTS AND DISCUSSION

A. Line tension and its sign

In the following parts, the characteristic length scale $x^* = 10^{-9}$m, the characteristic surface tension $\gamma^* = 10^{-2}$N$/m$, and the characteristic time $t^* = 10^{-9}$s are chosen to normalize all other physical parameters.

In this section, we first discuss the positive line tension of the sessile droplet on a flat substrate. The prefactor $s = 0$ in the wall energy density Eq. (10) is adopted. The effect of s on the immiscible gap between droplet and matrix molecules on the substrate is discussed later in Sec. III B. With increasing κ^* from 0 to 500, the apparent contact angle θ enlarges and deviates from θ_Y, as guided by the red dashed line in Fig. 2(a). Moreover, the linear relationship of $\cos\theta$ with $1/r^*$ shows good consistency with Eq. (14), as illustrated in Fig. 2(b).

In previous research, the negative line tension is an unsettled problem. Its existence is either proven by static equilibrium [5] with the sharp interface approach, or simulated with the molecular dynamics [14,25]. Here, we interpret the negative line tension based on thermodynamics and scrutinize its feasibility with the diffuse interface model which is more realistic for the submicro sessile droplet than the sharp interface approach. In literature [26,27], considerably larger

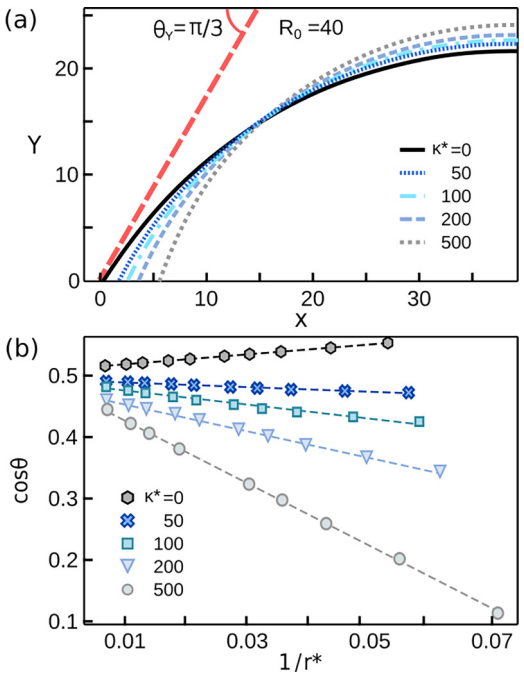

FIG. 2. The positive line tension effect for Young's contact angle $\theta_Y = \pi/3$. (a) The droplet silhouette with an initial droplet cap radius $R_0 = 40$ by different line tension parameters κ^*. (b) The cosine value of apparent contact angle θ with the contact line radius r^*. The dashed color lines are fitted with the modified Young's law, Eq. (14).

negative line tensions with several nJ$/m$ or even μJ$/m$ are reported and analyzed by setting the negative value of γ in the modified Young's law. However, from a mathematical point of view, a negative γ larger than several nJ$/m$ is unfeasible in our diffuse interface model. Expressed in the cylindrical coordinate, the wetting boundary condition yields

$$\tau \partial_t c = 2\kappa \nabla c \cdot \mathbf{n} - g' + 2\kappa^* \partial_r c/r + \partial_{rr} c). \tag{15}$$

By large negative line tension varying from -1.0nJ$/m$ to -1.0μJ$/m$, κ^* should be in the range of $-10^2 \sim -10^5$. Differing from the sharp interface model, Eq. (15) contains an additional Laplacian $2\kappa^* \partial_{rr} c$ which can easily lead to an ill-posed wetting boundary condition, and tiny composition fluctuation can give rise to instability at the triple junction. It is noteworthy that our model still captures the intrinsic negative line tension behavior. By setting line tension parameter $\kappa^* = 0$, see Fig. 3, the positive tendencies of $\cos\theta \sim 1/r^*$ with different θ_Y bear a resemblance to the characteristic of the negative line tension. Fitted with Eq. (14), the intrinsic line tension $\gamma_i = -0.5\sigma_{LV}$ is in the same magnitude as reported in [28]. For water drops at room temperature with $\sigma_{LV} = 0.072$ N$/m$, the minimal intrinsic line tension lays in $\gamma_i = -36$ pN which is in good conformity with Ref. [29].

To understand the intrinsic negative line tension, it is instructive to deliberate upon the distinction between the wetting boundary condition, Eq. (9), and the Cahn-Hilliard equation, Eq. (8). Notably, by setting $\kappa^* = 0$, the wetting boundary condition exclusively accounts for the compositional gradient in the normal direction of the substrate $\nabla c \cdot \boldsymbol{n}$, thereby disregarding the curvature effect on the substrate layer that is perpendicular to $\boldsymbol{n}$. In contrast, the material above the

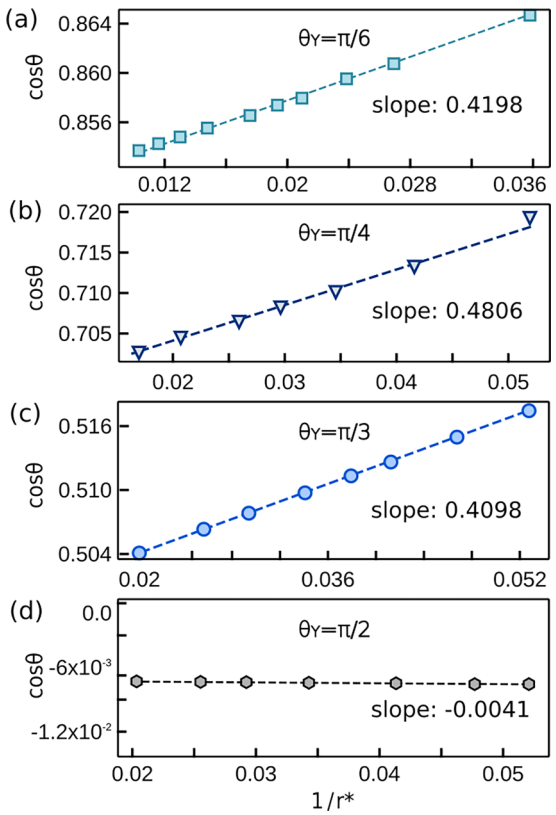

FIG. 3. The intrinsic negative line tension effect for different θ_Y by setting $\kappa^* = 0$. (a) $\theta_Y = \pi/6$; (b) $\theta_Y = \pi/4$; (c) $\theta_Y = \pi/3$; (d) $\theta_Y = \pi/2$.

substrate adheres to Eq. (8) and encompasses the curvature effect through the Laplacian term $-2\kappa\nabla^2 c$. Thus, within the substrate layer, the droplet-matrix interfacial tension γ corresponds to that of a planar interface, unaffected by curvature effects. While beyond the substrate layer, the interfacial tension exhibits dependence on curvature. This distinction suggests a discrete treatment of the substrate layer and the material above it, akin to the concept of the Gibbs dividing surface [4,5]. Despite the equilibrium condition within the entire domain, where all molecules possess an identical zero chemical potential, the chemical potential at the substrate is treated disregarding the curvature effect, deviating from that within the bulk. In this way, we suggest that the measured negative line tension is actually emanated from the curvature dependent chemical potential, which is in line with the Gibbs' adsorption. A deeper understanding on the negative line tension and Tolman length necessitates further investigation in our forthcoming research endeavors.

B. Wetting edge

Another salient feature encapsulated within our diffuse interface model pertains to the wetting edge observed at the triple junction of the droplet-matrix-substrate interface. This phenomenon has been substantiated through experimental studies [31,32]. Figure 4(a), adapted from Ref. [30], illustrates the alkane-air interface, where the measured profile (black dots) reveals a deviation from the idealized spherical shape (red line) at the triple junction. As highlighted by the dashed rectangles in Fig. 4(b), the increasing line tension effect, characterized by the parameter κ^*, accentuates the presence of a similar wetting edge in our simulations. To elucidate

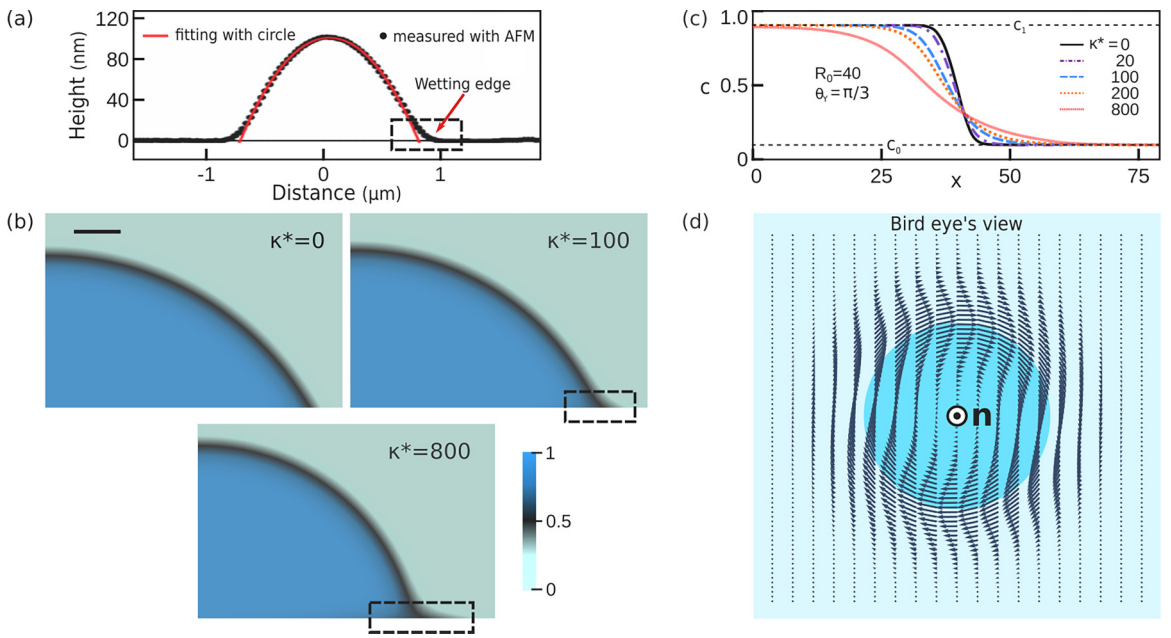

FIG. 4. (a) Atomic force microscopy profile of the alkane droplet (dots) deviating from the spherical fit (red line) at the triple junction. The wetting edge is highlighted in the dashed square, reproduced with permission from Ref. [30], copyright © 2003, American Physical Society. (b) The expanding wetting edge (highlighted in dashed squares) on the substrate with increasing the line tension parameters κ^*. The scale bar denotes ten and the color bar scales the droplet composition. (c) Droplet concentration c along the radial direction on the substrate S. (d) The schematic diffused line tension vector on S with a bird's eye view.

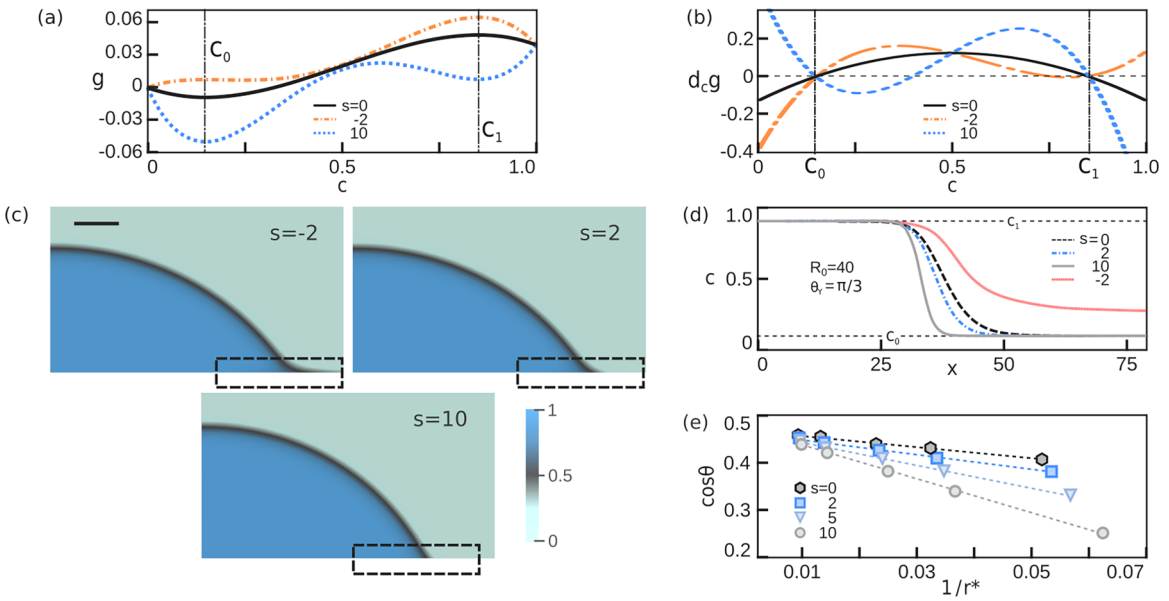

FIG. 5. The effect of wall energy on the line tension effect. (a) The wall energy $g(c)$ with the varying parameter s in Eq. (10). (b) The plot of dg/dc with varying s. (c) The shrinkage of the wetting edge (see dashed squares) with increasing s at $\kappa^* = 100$. (d) Composition profile along the radial direction on S. (e) Enhancing line tension effect with s. $\cos\theta$ versus $1/r^*$ for different s at $\kappa^* = 100$. The dashed color lines are fitted with Eq. (14).

the mechanism governing its formation, we examine the equilibrium composition of the droplet at the boundary layer spanning over the contact line, as portrayed in Fig. 4(c). This analysis reveals that an increase in line tension results in a flattening of the droplet-matrix interface on the substrate, thus implying that the altered concentration distribution across the contact line is highly associated with the manifestation of the wetting edge.

To comprehend the fundamental mechanism driving the concentration flattening on the substrate, a thorough examination of the mathematical formulation representing line tension in the diffuse interface model is imperative. In our approach, the line tension sprawls over a vector field that encompasses the entire wetting layer, as sketched in Fig. 4(d). This scenario is in remarkable contrast to the sharp interface model, wherein the line tension exclusively influences the sharp contact line. In this context, the diffused line tension effect arises from the sum of two distinct components within the integral, specifically denoted as $\int_{c_0}^{c_1} 2\kappa^*(\partial_r c)^2/r\, dc$ and $\int_{c_0}^{c_1} 2\kappa^*\partial_{rr}c\, dc$. The first term, reliant on gradient $\partial_r c$, serves to establish the equivalence between the sharp and diffuse interface formulations of line tension. The second integral, involving the Laplacian term $\partial_{rr}c$, becomes zero [see Eq. (12)], a feature absent in the sharp interface model. However, it is crucial to emphasize the significance of the Laplacian term $\partial_{rr}c$ in the differential form of Eq. (15). This term cannot be disregarded; rather, it assumes a diffusionlike formulation that facilitates the smoothing of compositional distribution across the contact line, as vividly depicted in Fig. 4(c). Consequently, to establish a local equilibrium state across the entirety of the substrate, the concentration profile c within the wetting layer is flattened by the Laplacian term $\partial_{rr}c$ scaled by κ^*, thereby giving rise to the manifestation of the wetting edge at the triple junction. Notably, this mechanistic facet remains unaccounted for in the sharp interface model.

Furthermore, from the thermodynamic point of view, we explain the wetting edge as the result of line energy minimization. The most common consensus is that the droplet reducing its contact line length $2\pi r^*$ is the only mechanism to decrease the line energy. So at equilibrium, an apparent contact angle larger than Young's angle θ_γ is reached. Here, we suggest the second mechanism for line energy minimization. Since the droplet-matrix interface on the substrate layer flattens with stronger line tension, a smaller $\partial_r c$ declines the line tension $\gamma = \int_0^\infty 2\kappa^*(\partial_r c)^2 dr$ accordingly. Physically, the lowering $\partial_r c$ also indicates that the line tension energy minimization enhances the mixing of droplet and matrix molecules at the triple junction.

In this way, we infer that the droplet-matrix interaction on the substrate plays a vital role. For the system with weak repulsive interactions, the droplet and matrix molecules can mix easily with each other, which reduces $\partial_r c$ to weaken the line tension and widen the wetting edge. Whereas the stronger repulsive force limits their mixture, boosts $\partial_r c$, and intensifies the line tension effect. In lieu of expanding the wetting edge, the line energy reduction shortens the contact line length and steepens the apparent contact angle θ. Then, we examine our deduction by changing the scaling parameter s in the wall energy density Eq. (10) to modify the droplet-matrix-substrate triple interaction strength. This approach is distinct from previous wall energy formulations [19] where only the droplet-substrate and matrix-substrate double interactions are considered. As depicted in Fig. 5(a), the parameter s can significantly change the miscibility of droplets with the matrix on the substrate. When $s > 0$, the double-well wall energy density $g(c)$ defines the huge immiscible gap, while $s < 0$, $g(c)$ becomes an inverted double-well potential which facilitates their mixing. Clearly noticeable in Figs. 5(b) and 5(c) at $\kappa^* = 100$, with an increase in s, the energy barrier between droplet and matrix molecules stacks up, leading to a thinner

wetting edge and stronger line tension effect. Consequently, the steeper relationship of $\cos\theta$ with $1/r^*$ in Fig. 5(d) shows a positive correlation with s. This indicates the two competing mechanisms promoting line energy minimization: (i) contact line length reduction increases apparent contact angle θ; (ii) line tension drop extends the wetting edge. Therefore, highly contrasted to the sharp interface approach, the line tension in our diffuse interface model is not solely decided by the line tension parameter κ^* itself, but also relies on the wall energy of the system. In other words, line tension is a triple-body problem dominated by droplet-matrix-substrate interactions.

IV. CONCLUSION

In conclusion, we present a diffuse interface model for the line tension of a sessile droplet. The free energy of the line tension is deduced in the diffuse interface method, which is compatible with previous sharp-interface models. In particular, we observe the intrinsic negative line tension in our diffuse interface approach which conforms with previous experiments. The line tension more negative than $1.0\,\mathrm{nJ}/m$ is not thermodynamically consistent due to the instability induced by the crucial Laplacian term in our model, which is overlooked in sharp interface models. In addition, a physical mechanism is found for the wetting edge formation at the droplet-matrix contact region which emerges from the competing line energy and wall energy minimization. We expect that our model will help to understand the behaviors of the nanobubbles and cells.

ACKNOWLEDGMENTS

H.D.Z. thanks the Gottfried-Wilhelm Leibniz Prize NE 822/31-1 of the German Research Foundation (DFG) for funding the research. F.W. is grateful to the VirtMat Project No. P09 "Wetting Phenomena" of the Helmholtz Association (MSE-Programme No. 43.31.02). The authors acknowledge support from the state of Baden-Württemberg through bwHPC.

APPENDIX A: ENERGY LAW

Considering the scenario where hydrodynamics is overwhelmed by the diffusion process and the velocity on the substrate S is zero, the time derivative of the free energy functional of mixture $\mathcal{F}$ is deduced as

$$\frac{\partial \mathcal{F}}{\partial t} = \int_\Omega \frac{\partial}{\partial t}[f(c)+\kappa(\nabla c)^2]d\Omega + \int_s \frac{\partial}{\partial t}[g(c)+\kappa^*(\nabla c)^2]dS,$$

in which the energy dissipation in the bulk region reads

$$\begin{aligned}
&\int_\Omega \frac{\partial}{\partial t}[f(c)+\kappa(\nabla c)^2]d\Omega \\
&= \int_\Omega \left[\frac{\partial f}{\partial c}\frac{\partial c}{\partial t} + 2\kappa\nabla c\cdot\frac{\partial(\nabla c)}{\partial t}\right]d\Omega, \\
&= \int_\Omega \left[\frac{\partial f}{\partial c}\frac{\partial c}{\partial t} + \nabla\cdot\left(2\kappa\nabla c\frac{\partial c}{\partial t}\right) - 2\kappa\nabla^2 c\frac{\partial c}{\partial t}\right]d\Omega, \\
&= \int_\Omega \left(\frac{\partial f}{\partial c} - 2\kappa\nabla^2 c\right)\frac{\partial c}{\partial t}d\Omega - \int_s 2\kappa\nabla c\cdot\boldsymbol{n}\frac{\partial c}{\partial t}\,dS. \quad \text{(A1)}
\end{aligned}$$

Besides, the wall energy decreases with time as

$$\begin{aligned}
\int_s \frac{\partial}{\partial t}[g(c)+\kappa^*(\nabla c)^2]dS &= \int_s \left[g'\frac{\partial c}{\partial t} + 2\kappa^*\nabla c\cdot\frac{\partial(\nabla c)}{\partial t}\right]dS, \\
&= \int_s \left(g' - 2\kappa^*\nabla_s^2 c\right)\frac{\partial c}{\partial t}\,dS. \quad \text{(A2)}
\end{aligned}$$

Combining Eqs. (A1) and (A2), we have

$$\frac{\partial \mathcal{F}}{\partial t} = \int_\Omega \mu\frac{\partial c}{\partial t}\,d\Omega + \int_s \mu_s\frac{\partial c}{\partial t}\,dS, \quad \text{(A3)}$$

in which the chemical potentials in bulk and substrate are defined as

$$\mu = \frac{\partial f}{\partial c} - 2\kappa\nabla^2 c, \quad \mu_s = -2\kappa\nabla c\cdot\boldsymbol{n} + g' - 2\kappa^*\nabla_s^2 c.$$

Here, the normal vector of domain Ω is represented by $\hat{\boldsymbol{n}}$ which is actually equivalent to $-\boldsymbol{n}$ on the substrate S. Meanwhile, the chemical potential in Ω is defined as $\mu = \partial_c f - 2\kappa\nabla^2 c$ and the substrate chemical potential reads $\mu_s = -2\kappa\nabla c\cdot\mathbf{n} + g' - 2\kappa^*\nabla_s^2 c$. Substituting the evolution equations Eqs. (8) and (9) into Eq. (A1), altogether with the no-flux boundary condition $\nabla\mu\cdot\boldsymbol{n} = 0$, the free energy function dissipates as

$$\begin{aligned}
\frac{d\mathcal{F}}{dt} &= \int_\Omega \mu\nabla\cdot(\mathcal{M}\nabla\mu)\,d\Omega + \int_s \mu_s(-\tau\mu_s)\,dS, \\
&= -\int_\Omega \mathcal{M}(\nabla\mu)^2 d\Omega - \int_s \tau\mu_s^2\,dS \leqslant 0.
\end{aligned}$$

At equilibrium, we have $\nabla\mu = 0$ inside the domain Ω, denoting the solution of the standard Cahn-Hilliard equation. On the substrate, $\mu_s = 0$ is the steady solution of the Allen-Cahn type wetting boundary equation Eq. (9).

APPENDIX B: SPHERICAL SUBSTRATE

For the spherical substrate, the substrate-related newly added energy terms are expressed in polar coordinate $(\boldsymbol{e}_r, \boldsymbol{e}_\theta, \boldsymbol{e}_\phi)$, and Eq. (5) can be written as

$$\begin{aligned}
&\int_\Omega (\kappa_1\hat{\nabla}c\cdot\boldsymbol{e}_r + 2\,\kappa^*\hat{\nabla}^2 c\,\hat{\nabla}c\cdot\boldsymbol{e}_r)\,d\Omega \\
&\quad = \int_\Omega \hat{\nabla}\cdot[\,g\,\boldsymbol{e}_r + \kappa^*(\hat{\nabla}c)^2\,\boldsymbol{e}_r]\,d\Omega, \\
&\quad = \int_s [\,g(c) + \kappa^*(\hat{\nabla}c)^2]\,dS,
\end{aligned}$$

where the gradient in polar coordinate is defined as $\hat{\nabla} := (\partial_r, \partial_\theta, \partial_\phi)$ and the Laplacian is expressed as $\hat{\nabla}^2 := \partial_r(r^2\partial_r)/r^2 + \partial_\theta(\sin\theta\,\partial_\theta)/(r^2\sin\theta) + \partial_{\phi\phi}/(r^2\sin^2\theta)$.

[1] A. Amirfazli and A. Neumann, Status of the three-phase line tension: A review, Adv. Colloid Interface Sci. **110**, 121 (2004).

[2] B. M. Law, S. P. McBride, J. Y. Wang, H. S. Wi, G. Paneru, S. Betelu, B. Ushijima, Y. Takata, B. Flanders, F. Bresme *et al.*, Line tension and its influence on droplets and particles at surfaces, Prog. Surf. Sci. **92**, 1 (2017).

[3] F. Wang, Y. Wu, and B. Nestler, Wetting effect on patterned substrate, Adv. Mater., **35** 2210745 (2023).

[4] J. W. Gibbs, *The Collected Works of J. Willard Gibbs*, Vol. III (Yale University Press, 1948), pp. 219–229.

[5] R. C. Tolman, Consideration of the gibbs theory of surface tension, J. Chem. Phys. **16**, 758 (1948).

[6] B. Widom, Line tension and the shape of a sessile drop, J. Phys. Chem. **99**, 2803 (1995).

[7] B. M. Law, Theory of nucleated wetting, Phys. Rev. Lett. **72**, 1698 (1994).

[8] H. Fan, Liquid droplet spreading with line tension effect, J. Phys.: Condens. Matter **18**, 4481 (2006).

[9] K. K. Rangharajan, K. J. Kwak, A. Conlisk, Y. Wu, and S. Prakash, Effect of surface modification on interfacial nanobubble morphology and contact line tension, Soft Matter **11**, 5214 (2015).

[10] S. Liu, A. Pandey, J. Duvigneau, J. Vancso, and J. H. Snoeijer, Size-dependent submerging of nanoparticles in polymer melts: Effect of line tension, Macromolecules **51**, 2411 (2018).

[11] A. J. García-Sáez, S. Chiantia, and P. Schwille, Effect of line tension on the lateral organization of lipid membranes, J. Biol. Chem. **282**, 33537 (2007).

[12] H. Krobath, B. Różycki, R. Lipowsky, and T. R. Weikl, Line tension and stability of domains in cell-adhesion zones mediated by long and short receptor-ligand complexes, PLoS One **6**, e23284 (2011).

[13] M. A. van Limbeek and J. R. Seddon, Surface nanobubbles as a function of gas type, Langmuir **27**, 8694 (2011).

[14] B. Zhao, S. Luo, E. Bonaccurso, G. K. Auernhammer, X. Deng, Z. Li, and L. Chen, Resolving the apparent line tension of sessile droplets and understanding its sign change at a critical wetting angle, Phys. Rev. Lett. **123**, 094501 (2019).

[15] R. J. Good and M. Koo, The effect of drop size on contact angle, J. Colloid Interface Sci. **71**, 283 (1979).

[16] F. Wang and B. Nestler, Wetting transition and phase separation on flat substrates and in porous structures, J. Chem. Phys. **154**, 094704 (2021).

[17] J. W. Cahn and J. E. Hilliard, Free energy of a nonuniform system. I. interfacial free energy, J. Chem. Phys. **28**, 258 (1958).

[18] H. Zhang, Y. Wu, F. Wang, F. Guo, and B. Nestler, Phase-field modeling of multiple emulsions via spinodal decomposition, Langmuir **37**, 5275 (2021).

[19] D. Jacqmin, Contact-line dynamics of a diffuse fluid interface, J. Fluid Mech. **402**, 57 (2000).

[20] P. Yue, C. Zhou, and J. J. Feng, Sharp-interface limit of the cahn–hilliard model for moving contact lines, J. Fluid Mech. **645**, 279 (2010).

[21] L. Onsager, Reciprocal relations in irreversible processes. I., Phys. Rev. **37**, 405 (1931).

[22] H. Zhang, F. Wang, and B. Nestler, Janus droplet formation via thermally induced phase separation: A numerical model with diffusion and convection, Langmuir **38**, 6882 (2022).

[23] P.-G. De Gennes, Wetting: Statics and dynamics, Rev. Mod. Phys. **57**, 827 (1985).

[24] F. Wang, H. Zhang, Y. Wu, and B. Nestler, A thermodynamically consistent diffuse interface model for the wetting phenomenon of miscible and immiscible ternary fluids, J. Fluid Mech. **970**, A17 (2023).

[25] J. H. Weijs, A. Marchand, B. Andreotti, D. Lohse, and J. H. Snoeijer, Origin of line tension for a lennard-jones nanodroplet, Phys. Fluids **23**, 022001 (2011).

[26] G. E. Yakubov, O. I. Vinogradova, and H.-J. Butt, Contact angles on hydrophobic microparticles at water–air and water–hexadecane interfaces, J. Adhes. Sci. Technol. **14**, 1783 (2000).

[27] Y. Gu, Drop size dependence of contact angles of oil drops on a solid surface in water, Colloids Surf., A **181**, 215 (2001).

[28] B. H. Tan, H. An, and C.-D. Ohl, Body forces drive the apparent line tension of sessile droplets, Phys. Rev. Lett. **130**, 064003 (2023).

[29] M. Kanduč, L. Eixeres, S. Liese, and R. R. Netz, Generalized line tension of water nanodroplets, Phys. Rev. E **98**, 032804 (2018).

[30] A. Checco, P. Guenoun, and J. Daillant, Nonlinear dependence of the contact angle of nanodroplets on contact line curvature, Phys. Rev. Lett. **91**, 186101 (2003).

[31] E. B. Webb III, G. S. Grest, and D. R. Heine, Precursor film controlled wetting of pb on cu, Phys. Rev. Lett. **91**, 236102 (2003).

[32] M. N. Popescu, G. Oshanin, S. Dietrich, and A. Cazabat, Precursor films in wetting phenomena, J. Phys.: Condens. Matter **24**, 243102 (2012).